ACS APPLIED MATERIALS & INTERFACES

Research Article

www.acsami.org

# Polymeric Micelle Assembly for the Direct Synthesis of Platinum-Decorated Mesoporous $TiO_2$ toward Highly Selective Sensing of Acetaldehyde

Bishnu Prasad Bastakoti,[†] Nagy L. Torad,[†,‡] and Yusuke Yamauchi*[,†,‡,§]

[†]World Premier International (WPI) Research Center for Materials Nanoarchitectonics (MANA), National Institute for Materials Science (NIMS), 1-1 Namiki, Tsukuba, Ibaraki 305-0044, Japan

[‡]Faculty of Science and Engineering, Waseda University, 3-4-1 Okubo, Shinjuku, Tokyo 169-8555, Japan

[§]Precursory Research for Embryonic Science and Technology (PRESTO), Japan Science and Technology Agency (JST), 4-1-8 Honcho, Kawaguchi, Saitama 332-0012, Japan

Supporting Information

**ABSTRACT:** Platinum-decorated mesoporous $TiO_2$ is synthesized by the self-assembly of polymeric micelles of an asymmetric triblock copolymer with three chemically distinct units in an acidic tetrahydrofuran solution. The strong hydrophobic interaction of platinum(II) 2,4-pentanedionate with a polystyrene core and electrostatic interaction of titanium tetraisopropoxide with a poly(vinylpyridine) shell enable us to directly synthesize crystalline mesoporous $TiO_2$ with platinum nanoparticles. A thermally stable block copolymer prevents collapse of the ordered mesostructure during the calcination process. The platinum source is in situ reduced to form the platinum nanoparticles on the $TiO_2$ walls. The sensing performance of platinum-decorated mesoporous $TiO_2$ is studied in detail using a quartz crystal microbalance technique, and it is found that it shows excellent sensitivity for acetaldehyde.

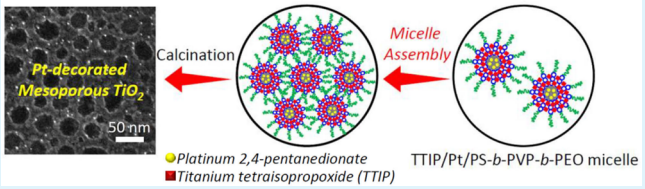


**KEYWORDS:** *micelle assembly, mesoporous $TiO_2$, platinum, sensor, acetaldehyde, quartz crystal microbalance*

## 1. INTRODUCTION

There is great interest in implementing a highly efficient sensor in order to improve environmental and safety control of pollutants. Several nanostructures, such as ZnS, CdSe, $TiO_2$, $SnO_2$, and ZnO, appear to be the best candidates for semiconductor sensors.[1−5] The sensitivity of these materials depends on their conductivity, porosity, and morphology. One of the widely used methods to increase the sensitivity and selectivity of the sensing efficiency of semiconductor sensors is the addition of some active metals, like platinum (Pt), palladium (Pd), and gold (Au).[6−10] The insertion of metal nanoparticles is believed to promote chemical and electronic sensitization.[11] Chemicurrent is observed when metal−semiconductor contacts are exposed to some reactive gases.[12,13] The strong interaction between $TiO_2$ and Pt has been found to favor the catalytic activities in fuel cells,[14] hydrogen production,[15] catalytic reduction of $CO_2$,[16] oxidation of hydrogen to water,[17] and sensing of different vapor organic compounds.[18,19]

As the widely used technologies for the insertion of metals (metal oxides), there are laser-induced pyrolysis,[20] sputtering,[21] sol−gel,[22] colloidal deposition,[23] photoirradiation,[24] and chemical vapor deposition.[25] Post-treatment of porous materials with metal nanoparticles is also a very common method to insert metal nanoparticles into or onto the framework.[26] However, multiple steps and complicated synthetic systems are required. Also, serious blocking of the pore by metal nanoparticles is sometimes observed, which drastically reduces the performance of the materials.

Like the previous examples, porous $TiO_2$ with Pt nanoparticles were synthesized using a photoassisted reduction method.[27] Pt/$TiO_2$ synthesized by a solvothermal method in oleic acid remarkably improved the response with respect to pure $TiO_2$ sensors over ethanol sensing.[28] A molten salt method was also adopted to introduce transition metals into $TiO_2$ nanowires.[29] Pt was encapsulated into ceria using a modified emulsion method. Oxidation of a ceric ion is coupled with reduction of $Pt^{4+}$ to Pt.[30] A macroporous $WO_3$ film with transition metals was also synthesized by a sol−gel approach with poly(methyl methacrylate) microspheres.[31] Many efforts have been made for the preparation of metal-decorated mesoporous $TiO_2$. In the previous systems, however, multiple steps are required in the synthesis.

In particular, mesoporous/nanoporous $TiO_2$ materials are very interesting because of their huge surface areas and large pore volumes, which can capture metal nanoparticles. The aim of this work is to develop our "polymeric micelles assembly"[32] to synthesize Pt-decorated mesoporous $TiO_2$ for enhanced

Received: September 14, 2013
Accepted: December 10, 2013
Published: December 27, 2013

  

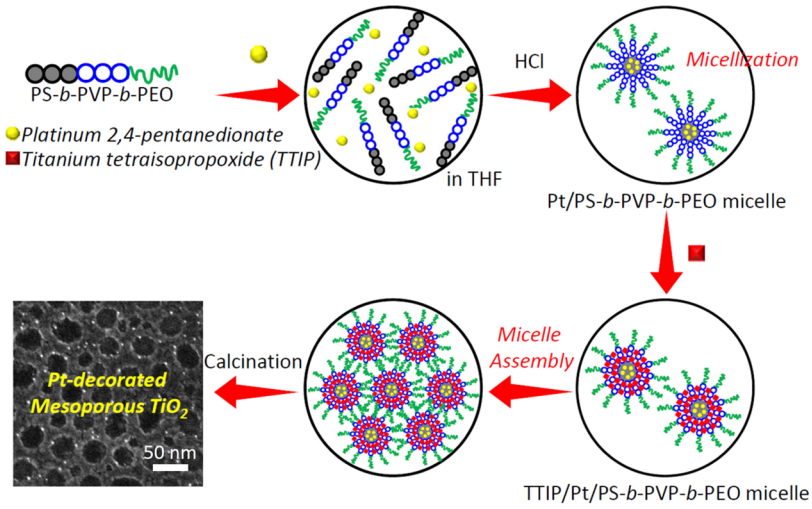


**Figure 1.** Illustration of the synthetic process of Pt-decorated mesoporous $TiO_2$ by "polymeric micelle assembly".

sensing efficiency over several organic molecules. The use of an asymmetric-type block copolymer [poly(styrene-*b*-2-vinylpyridine-*b*-styrene), PS-*b*-PVP-*b*-PEO] as a structure-directing agent can allow us to directly synthesize Pt-decorated mesoporous $TiO_2$. The hydrophobic interaction of platinum(II) 2,4-pentanedionate with the PS block and the electrostatic force of interaction between titanium tetraisopropoxide (TTIP) and the PVP block can allow one to successfully insert Pt nanoparticles inside the pore of mesoporous $TiO_2$. The sensing performance of Pt-decorated mesoporous $TiO_2$ is also studied in detail using a quartz crystal microbalance (QCM) technique, and the results reveal unusual high sensitivity to acetaldehyde.

## 2. EXPERIMENTAL SECTION

**2.1. Materials.** Titanium tetraisopropoxide (TTIP; Wako), platinum(II) 2,4-pentanedionate (Alfa Aesar), hydrochloric acid (HCl; Nacalai), tetrahydrofuran (THF; Wako), and several solvents [acetaldehyde, ethanol, acetone, ammonia, carbon tetrachloride ($CCl_4$), hexane, and benzene from Aldrich] were used without purification.

**2.2. Synthesis of Pt-Decorated Mesoporous $TiO_2$.** Here we used a $PS_{(14500)}$-*b*-$PVP_{(20000)}$-*b*-$PEO_{(33000)}$ triblock copolymer with polydispersity index 1.15 (the numbers in parentheses indicate the molecular weights of each block). The synthetic process is illustrated in Figure 1. Platinum(II) 2,4-pentanedionate (20 mg) was added to molecularly dissolved the PS-*b*-PVP-*b*-PEO block copolymer in THF. The final concentration of the polymer was 5 $g{\cdot}L^{-1}$. A concentrated HCl solution of 27% (100 $\mu$L) was slowly added to accelerate micellization (Pt/PS-*b*-PVP-*b*-PEO micelles). Then, TTIP (80 $\mu$L) was added and stirred for 3 h at room temperature (TTIP/Pt/PS-*b*-PVP-*b*-PEO micelles). The obtained solution was allowed to dry at room temperature. After complete evaporation of the solvent, the dried powder was collected and calcined at 600 °C in $N_2$ flow to remove the polymer template and induce crystallization of the pore walls. The applied calcination time was 3 h at a ramping rate of 1 $°C{\cdot}min^{-1}$. Finally, Pt-decorated mesoporous $TiO_2$ was obtained. For comparison, we also prepared pure mesoporous $TiO_2$ without Pt nanoparticles.

**2.3. Characterization of Pt-Decorated Mesoporous $TiO_2$.** Dynamic light scattering (DLS) measurements were carried out using an Otsuka ELS Z $\zeta$-potential and particle analyzer. All of the measurements were carried out at 25 °C. The morphology of the samples was observed by field-emission scanning electron microscopy (SEM; Hitachi SU-8000) and transmission electron microscopy (TEM; JEOL JEM-1210). The crystalline phases were investigated by powder X-ray diffraction (XRD) measurement (Shimadzu XRD-7000) analysis. Raman spectra were obtained by a Raman spectrometer (Jobin-Yvon T64000). Thermogravimetric analysis (TGA) was carried out using a SEIKO-6300 TG/DTA instruments at a heating rate of 10 $°C{\cdot}min^{-1}$ in $N_2$ flow. $N_2$ adsorption−desorption isotherms were obtained by a Quantachrom surface area analyzer.

**2.4. QCM Sensing Setup for Vapor Organic Compounds.** Prior to the film deposition process, QCM electrodes were first sonicated in a mixture of ethanol and water for 1 h. The electrodes were dried under a gentle stream of $N_2$ gas. The frequency was recorded as the initial frequency for the electrode ($F_0$). The $F_0$ value was used for measuring the mass of the sample coated on QCM electrodes according to the Sauerbrey equation (eq 1). The Pt-decorated mesoporous $TiO_2$ powder was dispersed in an aqueous solution of nafion (0.1 wt %). The final concentration of the sample was 1 $mg{\cdot}mL^{-1}$. The sample was coated onto the top surface of a QCM electrode by drop-coating at room temperature. After drying in a gentle $N_2$ flow, the electrode surface was rinsed with pure water and then continuously dried under vacuum for 2 h.

A 9 MHz AT-cut quartz crystal with Au electrode in both sides was used to measure the frequency. The schematic illustration of the QCM device is shown in Figure S1 in the Supporting Information. The QCM electrode coated with the sample was fixed inside a QCM instrument (QCA922; SEIKO EG&G Co. Ltd., Japan). Measurements were carried out in a sealed glass cell with an internal volume of 320 mL. A syringe was used for injection of chemical vapors (acetaldehyde, ethanol, acetone, ammonia, water, carbon tetrachloride, hexane, and benzene). Initially, a $N_2$ gas flow was passed over the cell to remove the humidified air. After recording the stable baseline ($\pm$1 $Hz{\cdot}min^{-1}$) for the modified QCM electrode in the glass cell, analytes with different concentrations were successively injected into the sealed glass cell. The time dependence of the frequency shift ($\Delta F$) was plotted during exposure of the injected analyte molecules. The frequency was automatically recorded by a PC-suppported program.

The QCM-based adsorption method offers the capability of acquiring real-time monitoring of the sorption processes of vapor molecules in the nanogram range. When a small amount of mass is adsorbed onto a quartz electrode surface, the frequency of the quartz is changed. By measurement of the frequency, the mass (per unit area) of the sample ($\Delta m$, $g{\cdot}cm^{-2}$) coated over the electrode can be calculated. Sauerbrey described the fractional decrease in the frequency of the oscillator upon deposition of a mass of material on its electrode surface.[33] The Sauerbrey equation is used to relate the frequency change ($\Delta F$) to the mass loading of the sample ($\Delta m$). The mass of the materials and frequency shift have an inverse relationship, as shown in the following equation:


dx.doi.org/10.1021/am4039954 | ACS Appl. Mater. Interfaces 2014, 6, 854−860

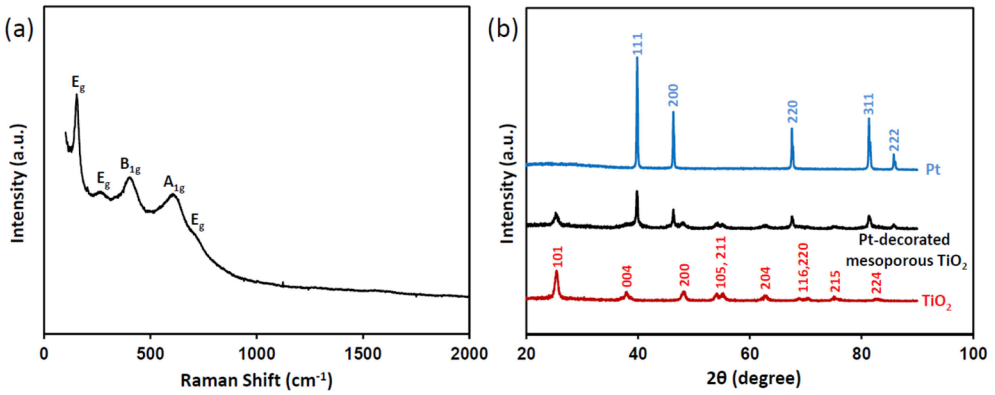


**Figure 2.** (a) Raman spectra of Pt-decorated mesoporous $TiO_2$ calcined at 600 °C in $N_2$ flow. (b) Wide-angle XRD patterns of Pt-decorated mesoporous $TiO_2$ calcined at 600 °C in $N_2$ flow. The XRD patterns of pure Pt nanoparticles and mesoporous $TiO_2$ are also shown for comparison.

$$\Delta F = -\frac{2F_0^2}{\sqrt{\rho\mu}}\frac{\Delta m}{A} \quad (1)$$

where $F_0$, $\rho$, $\mu$, and $A$ are the fundamental resonance frequency, crystal density (2.649 g·cm$^{-3}$), elastic modulus of the crystal ($2.947 \times 10^{11}$ g·cm$^{-1}$·s$^{-2}$), and surface area (0.196 cm$^2$), respectively. $\Delta F$ of the sample after drop-coating and drying-up was experimentally obtained as 6750.7 Hz. Thus, the sample amount coated onto the electrode was estimated to be 12.2 $\mu$g·cm$^{-2}$.

The gas-sensing property was measured using a static test system, with a sealed glass cell with an internal volume of 320 mL. A certain volume of liquid analytes was injected into the cell, and the vapor concentration was calculated using the following equation:[34]

$$C_{ppm} = \frac{22.4\rho T V_s}{273MV} \times 10^3 \quad (2)$$

where $C_{ppm}$ is the analyte concentration (ppm), $\rho$ is the density of the injected liquid analyte (g·mL$^{-1}$), $T$ is the temperature of the detection chamber (K), $V_s$ is the volume of the liquid sample ($\mu$L), $M$ is the molecular weight of the sample (g), and $V$ is the chamber volume (L).

Pt-decorated mesoporous $TiO_2$ influence the characteristic rate of uptake of vaporized acetaldehyde, which is controlled by diffusion, defined as $D/r^2$, where $D$ is the diffusion coefficient and $r$ is the diffusion length, which is controlled by the diffusion coefficient and surface area (geometry). Assuming that the surface concentration is always constant, the time dependence of the frequency shift ($\Delta F$) upon uptake of acetaldehyde vapor should be calculated. This constant surface concentration model is a simple linear model of adsorption commonly used in the literature, known as the Fickian model.[35] Thus, the solution of short-time ($t$) behavior can be described based on Fick's law for diffusion for a concentration into a homogeneous sphere of radius $r$, with $D$ being the diffusion coefficient inside the sphere.

$$\frac{\Delta F_t}{\Delta F_\infty} = 6\sqrt{\frac{D}{\pi}}\frac{t^{1/2}}{r^2} \quad (3)$$

where $\Delta F_t$ and $\Delta F_\infty$ are the frequency changes at any time $t$ and equilibrium state at the end of the adsorption process, respectively. The frequency change−time dependency is given by $\Delta F_t/\Delta F_\infty = (F_t - F)/(\Delta F_\infty - F)$, $F$ is the frequency of the electrode before injection at $t = 0$.

## 3. RESULTS AND DISCUSSION

**3.1. Synthesis of Pt-Decorated Mesoporous $TiO_2$.** PS-*b*-PVP-*b*-PEO block copolymer was first dissolved in THF, which is good solvent for all blocks. The synthetic process is illustrated in Figure 1. Platinum(II) 2,4-pentanedionate as a hydrophobic Pt source was added to the polymer solution. The Pt source was dissolved along with the polymer in THF. The formation of any micelles and/or aggregates was not observed by DLS measurement. A specific amount of a concentrated HCl solution was dropped slowly in order to initiate micellization. The HCl solution is a poor solvent for the PS block. Therefore, the interfacial energy between the PS block and the solvents is increased, leading to the formation of polymeric micelles in solution. The presence of micelles was immediately observed upon the addition of a HCl solution. The solution became slightly turbid. The comprehensive DLS experiment was performed to detect/measure the dimension of micelles. The average hydrodynamic diameter of the micelles was 100 nm, which was slightly larger than that of pure micelles (85 nm) without platinum(II) 2,4-pentanedionate. It has been reported, by the addition of the hydrophilic Pt source to the polymer solution, that the polystyrene domain swells and the interfacial area is increased.[36,37] The $\zeta$-potential remained unchanged, indicating that the addition of the Pt source cannot mask the surface charge of the polymeric micelles. Thus, the polymeric micelles were in an extended conformation. After the addition of TTIP, the $\zeta$-potential dramatically decreased from 35 to 5 mV, indicating the strong interaction of TTIP with the PVP block. As a result, the PVP shell showed a shrunken conformation. The hydrodynamic diameter was decreased to 55 nm. Intensity correlation curves of polymeric micelles with different components are shown in Figure S2a in the Supporting Information. TTIP/Pt/PS-*b*-PVP-*b*-PEO micelles exhibit faster diffusion curves compared to PS-*b*-PVP-*b*-PEO and Pt/PS-*b*-PVP-*b*-PEO micelles. These data indicate a higher diffusion coefficient and a lower hydrodynamic diameter. The morphology of TTIP/Pt/PS-*b*-PVP-*b*-PEO micelles was directly observed by SEM (Figure S2b in the Supporting Information). Every micelle was arranged without any aggregation. The average diameter of the micelles was measured to be about 45 nm, which was slightly smaller than the size measured by DLS. This is because the sample used in SEM observation is dry.

Heat treatment (in $N_2$ atmosphere at 600 °C for 3 h) simultaneously converted the amorphous $TiO_2$ framework into a highly crystalline $TiO_2$ framework, burned off the polymer template, and reduced the Pt precursor to Pt nanoparticles. It has been well-known that, when low-molecular-weight surfactants or pluronics-type block copolymers were used,[38−40] the crystallites grew and the original mesoporous structures easily collapsed or merged with each other during calcination. For example, weight loss of the P123 polymer started sharply at around 150 °C and was complete at 250 °C during TGA.[41] This temperature was a much lower temper-


dx.doi.org/10.1021/am4039954 | ACS Appl. Mater. Interfaces 2014, 6, 854−860

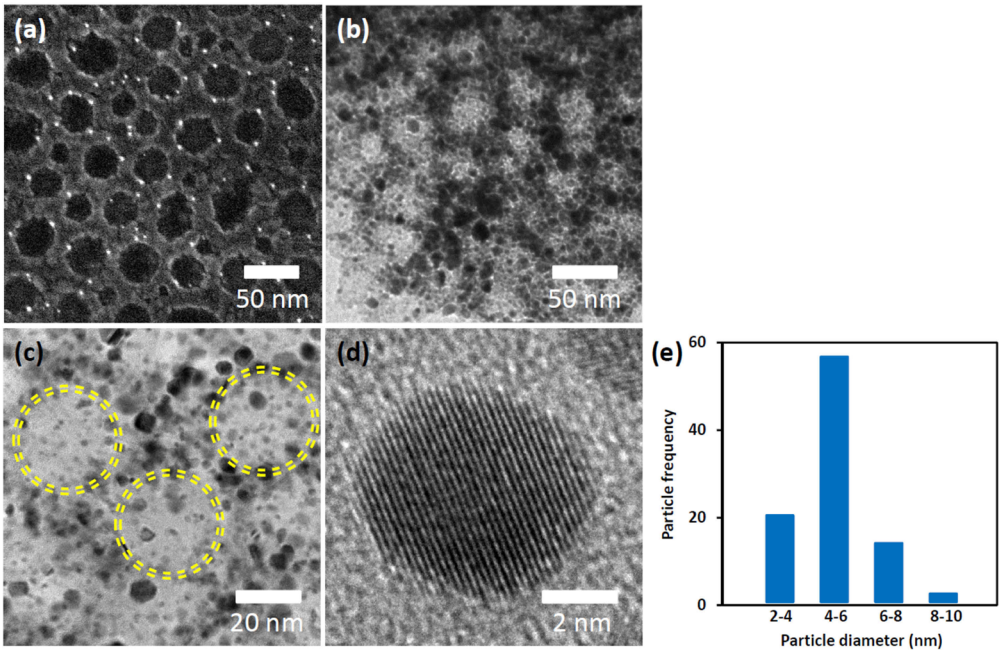


**Figure 3.** (a) SEM image and (b and c) TEM images of Pt-decorated mesoporous $TiO_2$ calcined at 600 °C in $N_2$ flow. (d) High-resolution TEM image of one Pt nanoparticle. (e) Particle-size distribution of Pt nanoparticles. Each mesopore is indicated by a yellow circle. Part c is the enlarged view of part b.

ature than the crystallization temperature of titania (about 350 °C). Thus, at temperatures higher than 250 °C, there were no templates to support the inorganic framework. Therefore, crystal growth was not suppressed, which led to collapse of the mesostructure.

In contrast, in our approach, the asymmetric-type block copolymer used in this study is thermally stable, which can protect the original mesoporous $TiO_2$ structure from collapse and further help in situ reduction of the platinum precursor. From the TGA curve of the polymer in $N_2$ flow (Figure S3 in the Supporting Information), a sharp weight loss was confirmed at around 450 °C, indicating complete combustion of the polymer. When the temperature reached 600 °C, the polymer derivatives (such as carbon) were completely removed. To ensure complete removal of the polymer derivatives, the sample was further investigated using Raman spectroscopy. The Raman spectrum of Pt-decorated mesoporous $TiO_2$ calcined at 600 °C is shown in Figure 2a. Any peaks derived from carbon were not observed. When the calcination temperature was 350 °C, two peaks derived from carbon were seen (Figure S4 in the Supporting Information). This temperature was not enough to remove the polymer. Upon an increase in the temperature up to 600 °C, the carbon peaks totally disappeared and the anatase peaks of $TiO_2$ became intense. Thus, the obtained Pt-decorated mesoporous $TiO_2$ calcined at 600 °C contained no carbon as well as no any other $TiO_2$ phase as the impurity. According to factor group analysis, the presence of five active modes (three $E_g$, $A_{1g}$, and $B_{1g}$) confirms the anatase phase of $TiO_2$.[42] The Raman spectrum of pure mesoporous $TiO_2$ is also shown for comparison (Figure S4 in the Supporting Information). The anatase peaks were more intense in pure mesoporous $TiO_2$ than Pt-decorated mesoporous $TiO_2$.

Figure 3a shows the SEM image of Pt-decorated mesoporous $TiO_2$. Calcination removes the polymer, leaving the $TiO_2$ framework with interconnecting spherical mesopores with an average diameter of 35−40 nm. The pore size corresponds to the void space formed after combustion of the polymer. The size of the pore is larger than that of the previously reported materials, which are synthesized from a similar block copolymer.[43] In a previous method, the polymer solution was prepared in aqueous solution, but here the presence of a large amount of THF helps to swell the PS core. As seen in Figure 3a−c, Pt nanoparticles were uniformly distributed into the mesoporous $TiO_2$. We can confirm that the platinum source hydrophobically interacts with the PS core because all of the Pt nanoparticles are inside the mesopores after removal of the polymeric template. Wiesner and co-workers also reported a one-pot synthesis method for the incorporation of metal nanoparticles (such as Pt, Pb, and PtPb) inside the pores of mesoporous $Nb_2O_5$ in which the hydrophobic metal source was mixed preferentially with a hydrophobic polyisoprene block.[44] Heating in an inert medium simultaneously crystallized $Nb_2O_5$, carbonized polyisoprene, and reduced metal precursors to metal nanoparticles. To gain more insight about the distribution of Pt nanoparticles, TEM observation was carried out. Parts b and c of Figure 3 show the TEM images of Pt-decorated mesoporous $TiO_2$. Figure 3c is the enlarged view of Figure 3b. The highly magnified TEM image of a single Pt nanoparticle (Figure 3d) revealed that it had coherently extended lattice fringes with a *d* spacing of 0.23 nm in agreement with the (111) plane of a face-centered-cubic (fcc) Pt crystal. The particle-size distribution of Pt nanoparticles is also shown in Figure 3e. More than 50% Pt nanoparticles were 4−6 nm in diameter. The Pt nanoparticles were strongly anchored on the surface of a robust $TiO_2$ wall. In order to further confirm the distribution of Pt nanoparticles in the mesoporous $TiO_2$, a high-angle annular dark-field scanning transmission electron microscopy (HAADF-STEM) image was taken (Figure S5 in the Supporting Information). It was clearly observed that the Pt nanoparticles were uniformly distributed on the pore walls.


dx.doi.org/10.1021/am4039954 | ACS Appl. Mater. Interfaces 2014, 6, 854−860

To obtain a realistic determination of the crystalline phase of Pt-decorated mesoporous $TiO_2$, wide-angle XRD measurement was carried out, as shown in Figure 2b. For comparison, XRD profiles of pure $TiO_2$ and Pt are also shown. All of the peaks of $TiO_2$ were exactly matched with the anatase form (JCPDS 00-021-1272), where as Pt is a fcc crystallite phase (JCPDS 04-0802). $N_2$ adsorption−desorption isotherms of Pt-decorated mesoporous $TiO_2$ is shown in Figure S6 in the Supporting Information. It is observed that the isotherm was of type IV and was representative of mesoporous materials. The surface area was found to be 48 $m^2 \cdot g^{-1}$.

**3.2. Sensing of Vapor Organic Compounds.** Several vapor organic compounds were tested to explore the potential application of Pt-decorated mesoporous $TiO_2$ as an excellent sensor in terms of higher sensitivity and fast response for chemical vapor detection using a QCM technique at room temperature. Acetaldehyde is a highly reactive and odorous organic compound and classified as a possible carcinogenic agent to humans by the International Agency for Research on Cancer of the World Health Organization.[45] Acetaldehyde is produced indoor and outdoor as a result of several anthropogenic activities.[46,47] Therefore, the increasing concern over environmental monitoring and safety demands in industry have generated great interest in the development and optimization of gas sensors with respect to their sensitivity, response rate, gas selectivity, and economic efficiency.[48−51] Here, our effort has been devoted to evaluate the acetaldehyde-sensing property, as well as to improve the sensor response, using a Pt-decorated mesoporous $TiO_2$-based film-coated QCM electrode. For this purpose, we fabricated a QCM sensor based on a Pt-decorated mesoporous $TiO_2$ powder with the aid of nafion as the binder (Figure S1 in the Supporting Information).

Figure 4a displays the dynamic response obtained upon exposure to acetaldehyde vapor with different concentrations ranging from 100 to 500 ppm. Upon each injection of acetaldehyde into the cell, the frequency of QCM accordingly underwent a decrease because of the large adsorption uptake of acetaldehyde molecules, which attained a steady value after several minutes. At a low acetaldehyde concentration of 100 ppm, QCM-based Pt-decorated mesoporous $TiO_2$ sensors exhibited higher adsorption uptake (frequency shift, $\Delta F$ = 416 Hz). Furthermore, the adsorption uptake of acetaldehyde remarkably increased with an increase of the injected concentration, which is quite consistent with the sensing behavior of n-type semiconductor sensors.[52] The maximum $\Delta F$ was 2307 Hz after 500 ppm injection. The response of QCM-based Pt-decorated mesoporous $TiO_2$ sensors increased exponentially and linearly with increasing concentration of injected acetaldehyde (from 100 to 500 ppm; Figure 4a). Here we confirmed a high detection sensitivity of 4.5 Hz·$ppm^{-1}$ and a lower limit of detection equal to 27 ppm. In contrast, when a QCM-based mesoporous $TiO_2$ sensor without Pt nanoparticles was used, low responsibility was observed. After injection of 100 ppm acetaldehyde, the adsorption uptake was only 156 Hz, as shown in the inset image of Figure 4a. Thus, compared to mesoporous $TiO_2$ without Pt nanoparticles, a Pt-decorated mesoporous $TiO_2$-based sensor provided almost 2.5 times higher uptake for acetaldehyde vapors. This result is easily attributed to the presence of metallic Pt, which remarkably enhances the sensing property because of the chemical sensitization mechanism. The presence of Pt nanoparticles not only provides abundant adsorption sites for the incoming

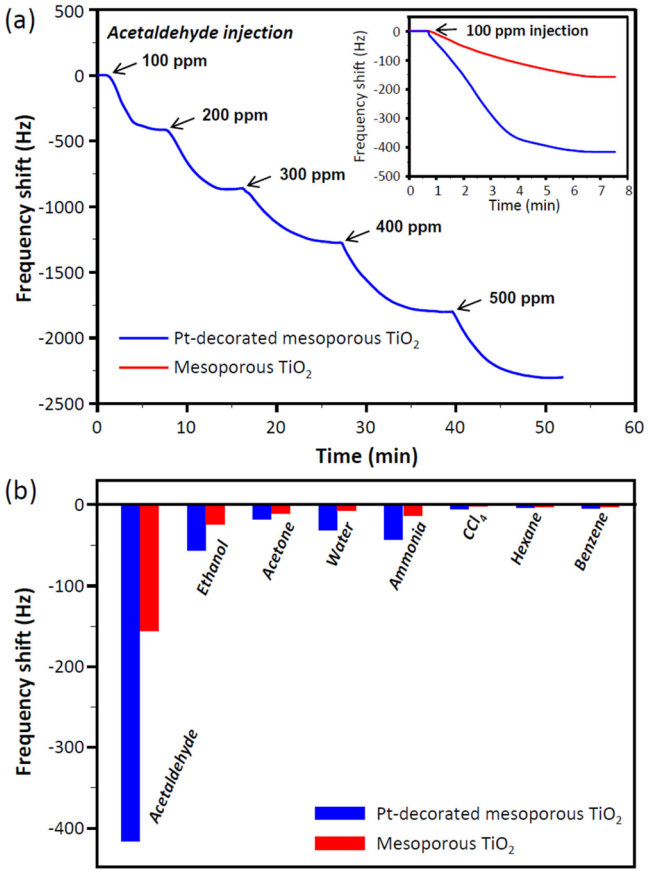


**Figure 4.** (a) Typical mass-normalized time-dependent frequency shift ($\Delta F$) curve of QCM coated with pure mesoporous $TiO_2$ (red line) and Pt-decorated mesoporous $TiO_2$-based films (blue line) caused by exposure to different injected concentrations of vaporized acetaldehyde. (b) Summary of QCM frequency shifts of mesoporous $TiO_2$-based films (red line) and Pt-decorated mesoporous $TiO_2$-based films (blue line) caused by exposure to various vaporized gases at 100 ppm.

gas molecules but also helps the spillover of oxygen species onto the $TiO_2$ surface, where they get ionosorbed by trapping electrons from $TiO_2$ (dipole−dipole interaction with the oxygen surface of $TiO_2$).[18,28,52]

It is very interesting to know that the Pt-decorated mesoporous $TiO_2$-based sensor has the highest affinity for acetaldehyde molecules among other possible interference gases such as ethanol, acetone, ammonia, water, $CCl_4$, hexane, and benzene at room temperature. The selective detection of acetaldehyde can be clearly realized. As is clearly observed in Figure 4b, the sensor was not sensitive to other toxic organic vapors, such as $CCl_4$, hexane, and benzene. In contrast, the mesoporous $TiO_2$-based sensor presented poor sensitivity for the chemical vapors, compared to Pt-decorated mesoporous $TiO_2$. These results revealed the unusually high sensitivity of the Pt-decorated mesoporous $TiO_2$ sensor to acetaldehyde. This high response and high selectivity would be attributed to the intrinsic reactivity of the target gas molecules and their diffusivities. To simplify our results, we also show the relative frequency shift of Pt-decorated mesoporous $TiO_2$ for different target gas molecules (Figure S7 in the Supporting Information). The sensitivity toward acetaldehyde is 7 times greater than than toward ethanol. The results indicate that the sensitivity of our material toward acetaldehyde is amazingly better than that of other tested target molecules.


dx.doi.org/10.1021/am4039954 | ACS Appl. Mater. Interfaces 2014, 6, 854−860

In previous reports, it was reported that the presence of metallic Pt can also increase the rate of uptake of adsorbed gas molecules.[18,19,53] In this study, the vapor adsorption kinetics was investigated by real-time monitoring of the frequency change of the QCM using Fick's law.[35] The experimental data were analyzed, and a plot of $\Delta F_t/\Delta F_\infty$ against $t^{1/2}$ is illustrated in Figure 5. A satisfactory linear fit for the obtained

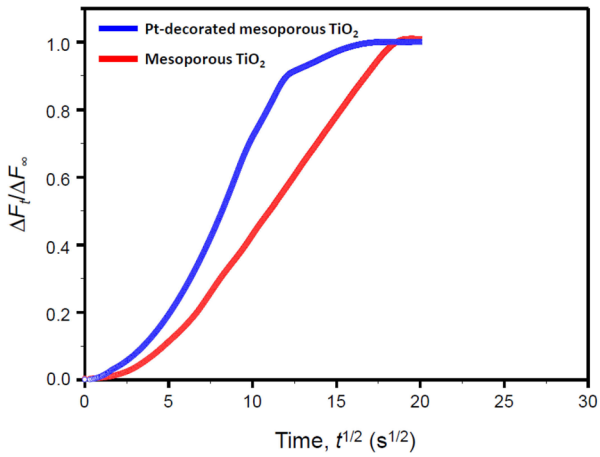


**Figure 5.** Graph of $\Delta F_t/\Delta F_\infty$ against $t^{1/2}$ for the uptake of acetaldehyde vapors (at 100 ppm injection) for pure mesoporous $TiO_2$ (red line) and Pt-decorated mesoporous $TiO_2$-based (blue line) thin films.

experimental data allows $D/r^2$ to be calculated from the linear regression of the slope; $D/r^2 = 1.3 \times 10^{-4}$ and $2.4 \times 10^{-4}$ $s^{-1}$ for mesoporous $TiO_2$ and Pt-decorated mesoporous $TiO_2$-based films, respectively. As is clearly indicated, the rate of uptake of acetaldehyde vapor into the Pt-decorated mesoporous $TiO_2$-based film was almost 2 times higher than that into mesoporous $TiO_2$ without Pt. From theoretical calculations (Figure 5), it was further demonstrated that acetaldehyde adsorption into a Pt-decorated mesoporous $TiO_2$-based film proceeds more rapidly than that of pure mesoporous $TiO_2$. Desorption of acetaldehyde molecules from a Pt-decorated mesoporous $TiO_2$-based film was also tested. Almost all of the acetaldehyde molecules were rapidly desorbed from the film (within a few minutes) after purging of $N_2$ gas inside the testing glass cell at room temperature. The good reversibility of our sensor will be very helpful for practical use in gas-sensing devices.

## 4. CONCLUSION

We synthesized Pt-decorated mesoporous $TiO_2$ by the self-assembly of an asymmetric triblock copolymer in an acidic THF solution. Because of the strong interaction of TTIP with polymeric micelles, the robust wall around the uniform large pores was formed. The hydrophobic interaction of the Pt source with the PS block enables us to successfully incorporate the Pt nanoparticles inside the pore. Our approach based on "polymeric micelle assembly" is a very simple and one-pot synthesis method. Also, there are several advantages of forming uniformly dispersed Pt nanoparticles inside as well as on the wall without serious aggregation, which is often considerable a challenge in nanoparticle synthesis. The sensitivity of Pt-decorated mesoporous $TiO_2$ toward acetaldehyde was 7 times greater than that toward ethanol and far better than that toward other tested molecules. This superior affinity of QCM-based Pt-decorated mesoporous $TiO_2$ sensors for acetaldehyde is a very promising result for highly selective detection, demonstrating a high potential for environmental monitoring and safety systems.

## ■ ASSOCIATED CONTENT

### Supporting Information

DLS, SEM, TEM, EDX, TGA, and BET data. This material is available free of charge via the Internet at http://pubs.acs.org.

## ■ AUTHOR INFORMATION

### Corresponding Author

*E-mail: Yamauchi.Yusuke@nims.go.jp. Homepage: http://www.yamauchi-labo.com.

### Notes

The authors declare no competing financial interest.

## ■ ACKNOWLEDGMENTS

This research is supported by the Japan Society for the Promotion of Science.

## ■ REFERENCES

(1) Kuang, Q.; Lao, C.; Wang, Z. L.; Xie, Z.; Zheng, L. *J. Am. Chem. Soc.* **2007**, *129*, 6070−6071.
(2) Spencer, M. J. S. *Prog. Mater. Sci.* **2012**, *57*, 437−486.
(3) He, J. H.; Zhang, Y.; Liu, Y. J.; Moore, D.; Bao, G.; Wan, Z. L. *J. Phys. Chem. C* **2007**, *111*, 12152−12156.
(4) Nazzal, A. Y.; Qu, L.; Peng, X.; Xiao, M. *Nano Lett.* **2003**, *3*, 819−822.
(5) Markus, M.; Lunkenbein, T.; Schieder, M.; Groschel, A. H.; Miyajima, N.; Fortsch, M.; Breu, J.; Caruso, F.; Muller, A. H. E. *Macromolecules* **2012**, *45*, 6981−6988.
(6) Xi, G.; Ye, J.; Ma, Q.; Su, N.; Bai, H.; Wang, C. *J. Am. Chem. Soc.* **2012**, *134*, 6508−6511.
(7) Redel, E.; Arsenault, E.; O'Brien, P. G.; Kherani, N. P.; Ozin, G. A. *Chem. Mater.* **2011**, *23*, 1353−1355.
(8) Zhang, Y.; Zheng, Z.; Yang, F. *Ind. Eng. Chem. Res.* **2010**, *49*, 3539−3543.
(9) Cho, N. G.; Woo, H.-S.; Lee, J.-H.; Kim, II-D. *Chem. Commun.* **2011**, *47*, 11300−11302.
(10) Yu, A.; Liang, Z.; Cho, J.; Caruso, F. *Nano Lett.* **2003**, *3*, 1203−1207.
(11) Yamazoe, N.; Kurokawa, Y.; Seiyama, T. *Sens. Actuators B* **1993**, *4*, 283−289.
(12) Nienhaus, H. *Surf. Sci. Rep.* **2002**, *45*, 1−78.
(13) Dasari, S. K.; Hashemian, M. A.; Mohan, J.; Karpov, E. G. *Chem. Phys. Lett.* **2012**, *553*, 47−50.
(14) Huang, S. Y.; Ganesan, P.; Park, S.; Popov, B. N. *J. Am. Chem. Soc.* **2009**, *131*, 13898−13899.
(15) Galinska, A.; Walendziewski, J. *Energy Fuels* **2005**, *19*, 1143−1147.
(16) Wang, C.; Thompson, R. L.; Baltrus, J.; Matranga, C. *J. Phys. Chem. Lett.* **2010**, *1*, 48−53.
(17) Karpov, E. G.; Dasari, S. K.; Hashemian, M. A. *J. Phys. Chem. C* **2013**, *117*, 15632−15638.
(18) Francioso, L.; Presicce, D. S.; Siciliano, P.; Ficarella, A. *Sens. Actuators B* **2007**, *123*, 516−521.
(19) Ponce, M. A.; Parra, R.; Savub, R.; Joanni, E.; Bueno, P. R.; Cilense, M.; Varela, J. A.; Castro, M. S. *Sens. Actuators B* **2009**, *139*, 447−452.
(20) Karhunen, T.; Lähde, A.; Leskinen, J.; Büchel, R.; Waser, O.; Tapper, U.; Jokiniem, J. *Nanotechnology* **2011**, 1−6.
(21) McCann, M. T. P.; Mooney, D. A.; Rahman, M.; Dowling, D. P.; Don MacElroy, J. M. *ACS Appl. Mater. Interfaces* **2011**, *3*, 252−260.
(22) Xie, Y.; Ding, K.; Liu, Z.; Tao, R.; Sun, Z.; Zhang, H.; An, G. *J. Am. Chem. Soc.* **2009**, *131*, 6648−6649.

(23) Comotti, M.; Li, W.-C.; Spliethoff, B.; Schuth, F. *J. Am. Chem. Soc.* **2006**, *128*, 917−924.
(24) Bastakoti, B. P.; Wu, K. C.-W; Yamauchi, Y. *J. Nanosci. Nanotechnol.* **2013**, *13*, 2735−2739.
(25) Zhang, Y.; Zhang, L.; Zhou, C. *Acc. Chem. Res.* **2013**, *46*, 2329−2339.
(26) Shanugam, S.; Gedanken, A. *J. Phys. Chem. C* **2009**, *113*, 18707−18712.
(27) Tian, M.; Wu, G.; Chen, A. *ACS Catal.* **2012**, *2*, 425−432.
(28) Epifani, M.; Andreu, T.; Zamani, R.; Arbiol, J.; Comini, E.; Siciliano, P.; Faglia, G.; Morante, J. R. *CrystEngComm* **2012**, *14*, 3882−3887.
(29) Liu, B.; Chen, H. M.; Liu, C.; Andrews, S. C.; Hahn, C.; Yang, P. *J. Am. Chem. Soc.* **2013**, *135*, 9995−9998.
(30) Yeung, C. M. Y.; Yu, K. M. K.; Fu, Q. J.; Thompsett, D.; Petch, M. I.; Tsang, S. C. *J. Am. Chem. Soc.* **2005**, *127*, 18010−18011.
(31) Arienzo, M. D.; Armelao, L.; Mari, C. M.; Polizzi, S.; Ruffo, R.; Scotti, R.; Morazzoni, F. *J. Am. Chem. Soc.* **2011**, *133*, 5296−5304.
(32) Bastakoti, B. P.; Ishihara, S.; Leo, S. Y.; Ariga, K.; Wu, K. C.-W.; Yamauchi, Y. *Langmuir*, Accepted.
(33) Sauerbrey, G. *Z. Phys.* **1959**, *155*, 206−222.
(34) Ayad, M. M.; El-Hefnawey, G.; Torad, N. L. *J. Hazard. Mater.* **2009**, *168*, 85−88.
(35) Crank, J. *The Mathematics of Diffusion*, 2nd ed.; Clarendon Press: Oxford, U.K., 1975; p 414.
(36) Lei, L.; Gohy, J.-F.; Willet, N.; Zhang, J.-X.; Varshney, S.; Jérôme, R. *Polymer* **2004**, *45*, 4375−4381.
(37) Bastakoti, B. P.; Guragain, S.; Yoneda, A.; Yokoyama, Y.; Yusa, S.; Nakashima, K. *Polym. Chem.* **2010**, *1*, 347−353.
(38) Kondo, J. N.; Domen, K. *Chem. Mater.* **2008**, *20*, 835−847.
(39) Lin, H. P.; Mou, C-Y *Microporous Mesoporous Mater.* **2002**, *55*, 69−80.
(40) Cejka, J. *Appl. Catal., A* **2003**, *254*, 327−238.
(41) Zakaria, M. B.; Suzuki, N.; Torad, N. L.; Matsuura, M.; Maekawa, K.; Tanabe, H.; Yamauchi, Y. *Eur. J. Inorg. Chem.* **2013**, 2330−2335.
(42) Tian, F.; Zhang, Y.; Zhang, J.; Pan, C. *J. Phys. Chem. C* **2012**, *116*, 7515−7519.
(43) Bastakoti, B. P.; Imura, M.; Nemoto, Y.; Yamauchi, Y. *Chem. Commun.* **2012**, *48*, 12091−12093.
(44) Orilall, M. C.; Matsumoto, F.; Zhou, Q.; Sai, H.; Abruna, H. D.; DiSalvo, F. J.; Wiesner, U. *J. Am. Chem. Soc.* **2009**, *131*, 9389−9395.
(45) *IARC Monographs on the Evaluation of Carcinogenic Risks to Humans*; WHO-IARC: Lyon, France, 1999; Vol. *71*, pp 14−18.
(46) Pesis, E.; Dvir, O.; Feygenberg, O.; Arie, R. B.; Ackerman, M.; Lichter, A. *Postharvest Biol. Technol.* **2002**, *26*, 157−165.
(47) Choodum, A.; Thavarungkul, P.; Kanatharana, P. *J. Environ. Sci. Health, Part B* **2007**, *45*, 577−583.
(48) Xu, P.; Yu, H.; Li, X. *Anal. Chem.* **2011**, *83*, 3448−3454.
(49) Li, C. C.; Yin, X. M.; Wang, T. H.; Zeng, H. C. *Chem. Mater.* **2009**, *21*, 4984−4992.
(50) Hu, M.; Reboul, J.; Furukawa, S.; Torad, N. L.; Ji, Q.; Srinivasu, P.; Ariga, K.; Kitagawa, S.; Yamauchi, Y. *J. Am. Chem. Soc.* **2012**, *134*, 2864−2867.
(51) Torad, N. L.; Hu, M.; Kamachi, Y.; Takai, K.; Imura, M.; Naito, M.; Yamauchi, Y. *Chem. Commun.* **2013**, *49*, 2521−2523.
(52) Zhang, M.; Yuan, Z.; Song, J.; Zheng, C. *Sens. Actuators B* **2010**, *148*, 87−92.
(53) Falconer, J. L.; Magrini-Bair, K. A. *J. Catal.* **1998**, *179*, 171−178.